Original Article

Risk assessment of severe postpartum hemorrhage after invasive placenta accreta based on three-dimensional reconstruction of magnetic resonance imaging

Liqun Liu[1#], Xiaoli Yan[1#], Jingjing Liu[2], Ping Yan[1], Mingshan Du[3], Runyuan Wang[2], Yi Wu[2], Dan Wang[1]

[1]Department of Obstetrics and Gynecology, Southwest Hospital, Army Medical University (Third Military Medical University), Chongqing, China; [2]Department of Digital Medicine, College of Biomedical Engineering and Medical Imaging, Army Medical University (Third Military Medical University), Chongqing, China; [3]Department of Radiology, Southwest Hospital, Army Medical University (Third Military Medical University), Chongqing, China

Contributions: (I) Conception and design: Y Wu, D Wang, L Liu; (II) Administrative support: Y Wu, D Wang; (III) Provision of study materials or patients: L Liu, X Yan, M Du; (V) Collection and assembly of data: L Liu, J Liu, P Yan; (IV) Data analysis and interpretation: J Liu, Y Wu, X Yan, R Wang; (V) Manuscript writing: All authors; (VI) Final approval of manuscript: All authors.

[#]These authors contributed equally to this work.

Correspondence to: Yi Wu. Department of Digital Medicine, Biomedical Engineering and Medical Imaging College, Army Medical University (Third Military Medical University), Chongqing 400038, China. Email: wuy1979@tmmu.edu.cn; Dan Wang. Department of Obstetrics and Gynecology, Southwest Hospital, Army Medical University (Third Military Medical University), Chongqing 400038, China. Email: swhwang@163.com.

Background: The aim of this study was to investigate the significance and feasibility of risk assessments based on the three-dimensional (3D) reconstruction of magnetic resonance imaging (MRI) of invasive placenta accreta (IPA) to create individualized surgical protocols and perioperative management plans in late pregnancy.

Methods: MRI and clinical data of 36 pregnant women with IPA admitted to Southwest Hospital from January 2017 to June 2021 were retrospectively analyzed. The patients were divided into the following 4 groups: peripartum hysterectomy (PH), abdominal aortic balloon block (AABB), PH with AABB, and nonsurgical treatment. Each group was then divided into severe and nonsevere postpartum hemorrhage subgroups based on postpartum hemorrhage volumes of not more than 2,000 mL and more than 2,000 mL, respectively. The uteri, placentas, IPA, and urinary bladders in each group were segmented and 3-dimensionally reconstructed using Amira 5.2.2 (Visage Imaging, Richmond, Australia) software, and their surface areas and volumes were calculated. A multifactorial unconditional logistic regression analysis was performed to evaluate the 3D morphological parameters of postpartum hemorrhage and calculate the optimal threshold.

Results: The bleeding volume, IPA area, placental area:uterine area ratio, IPA area:placental area ratio, maximum depth of IPA, placental position score, IPA position score, and implantation volume were greater in the severe postpartum hemorrhage subgroup than in the nonsevere postpartum hemorrhage subgroup of all groups. In the multifactorial regression analysis, the areas under the receiver operating characteristic curve of the implantation area, implantation volume, maximum depth of implantation, and implantation area:placental area ratio exceeded 0.9 and correlated strongly with severe postpartum hemorrhage, while those of the uterine area, uterine volume, placental area, placental volume, and placental area:uterine area ratio were between 0.5 and 0.7 and correlated with severe postpartum hemorrhage. The threshold (cutoff values) determining severe postpartum hemorrhage were 20,286.25 mm^2 of the implantation area, 0.01271 of the implantation area:placental area ratio, 15.03 mm of the maximum depth of implantation, and 46,846 mm^3 of the implantation volume.

Conclusions: The MRI 3D reconstruction of IPA and its adjacent structures can accurately display the location, anatomical morphology, and spatial relationship of IPA, which can be used to improve the accuracy of IPA diagnosis, predict postpartum hemorrhage, and provide optimized treatment decisions for

obstetricians.

Keywords: Magnetic resonance imaging (MRI); 3D reconstruction; placenta accreta spectrum; invasive placenta accreta; risk assessment

Submitted Jun 04, 2022. Accepted for publication Oct 08, 2022. Published online Jan 10, 2023.
doi: 10.21037/atm-22-2940
View this article at: https://dx.doi.org/10.21037/atm-22-2940

Introduction

Placenta accreta spectrum (PAS) is a term used to describe abnormal placental invasion, a clinical situation in which the placenta does not separate spontaneously at delivery and cannot be removed without causing abnormal and potentially life-threatening bleeding (1). PAS includes placenta accreta (penetration <0% of the myometrium), increta (penetration >50% of the myometrium), and percreta (penetration beyond the myometrium to the uterine serosa and adjacent organs). Placenta increta and percreta are collectively called "invasive placenta accreta" (IPA) (2). The risk of postpartum hemorrhage is particularly high in women with IPA (3) and associated with 40–60% of perioperative hysterectomies. (4) Inaccurate assessment of the presence or prognosis of IPA leads to its improper management and can cause severe uncontrollable postpartum hemorrhage and even death in pregnant women (5). However, accurate assessment of the bleeding risk in pregnant women with IPA, particularly in late pregnancy, requires stratified management, high-quality pregnancy care, appropriate treatment planning, and appropriate timing and planning of pregnancy termination to ensure maternal and infant safety (6).

Imaging examinations play a pivotal role in the diagnosis of IPA. Ultrasound is widely performed for clinical diagnosis, owing to its advantages of safety, cost-effectiveness, fast results, and convenience (7). Unlike ultrasound, prenatal magnetic resonance imaging (MRI) is less affected by intestinal gas, body size, and bone (8,9). Owing to the absence of ionizing radiation, thin-layer MRI is considered to be as safe as ultrasound in late pregnancy (10). However, both ultrasound and 2D MRI lack quantitative indicators for the diagnosis or grading of IPA, as they can barely display the detailed anatomical location, morphology, and spatial relationship of the IPA, placenta, and uterus. The 3D parameters, including IPA area, implantation volume, and implantation depth, are also not quantitatively described (11,12). Thus, misdiagnosis can easily occur.

Although many studies on the 3D reconstruction of IPA have suggested that the depth, area, and extent of IPA are closely related to postpartum hemorrhage (13-15), they have not clearly demonstrated the anatomical location, 3D morphology, or spatial relationship of IPA lesions. Mulligan *et al.* reported on the 3D reconstruction of the MRI of IPA with advantages in demonstrating the depth, extent, and location of IPA. Yet, even though the depth was roughly delineated according to the degree of invasion of the myometrium and the plasma layer of the uterus, the measurement of the length and width of abnormal placental implantation and the classification of abnormal placental implantation were only achieved in 2D (16), and no accurate numerical measurements related to IPA were performed. Moreover, the accuracy of these studies remains controversial, and whether implantation parameters including the IPA depth, area, and volume are related to postpartum hemorrhage remains unknown.

The aim of this retrospective study was to introduce a preoperative prediction method for pregnant women with IPA to assess the risk of postpartum hemorrhage using MRI 3D reconstruction of the IPA, placenta, uterus, and bladder, with the aim to create a guideline or decision-making protocol for the preoperative surgical planning of cesarean section for IPA. We present the following article in accordance with the STARD reporting checklist (available at https://atm.amegroups.com/article/view/10.21037/atm-22-2940/rc).

Methods

General data

The MRI and clinical data of 36 pregnant women with IPA admitted to Southwest Hospital from January 2017 to June 2021 were retrospectively analyzed. *Table 1* shows the basic information of patients with IPA. Imaging data included dynamic pelvic MRI in the sagittal, coronal, and horizontal

Table 1 Comparison of baseline data between the severe and non-severe postpartum hemorrhage subgroups

Group	Height (cm)	Weight (kg)	Age (years)	Number of pregnancies	Number of deliveries	Number of previous cesarean deliveries	Gestational week of termination of pregnancy	Duration of surgery (min)	Number of cleanings
Severe postpartum hemorrhage subgroup	156.00±3.39	65.66±8.96	31.88±4.18	4.13±1.36	2.31±0.79	1.38±0.62	35.70±1.30	146.38±48.95	1.56±1.31
Non-severe postpartum hemorrhage subgroup	156.65±3.92	69.75±12.71	32.35±4.83	5.40±2.16	2.50±0.76	1.60±0.75	36.19±1.60	182.70±55.02	2.55±2.28
P value	0.383	0.435	0.340	0.278	0.945	0.194	0.208	0.750	0.440

planes. The patients were further divided into the following 4 groups: peripartum hysterectomy (PH), abdominal aortic balloon block (AABB), PH with AABB, and nonsurgical treatment. Each group was divided into the following 2 subgroups according to the postpartum hemorrhage volume: the severe postpartum hemorrhage group, defined as postpartum bleeding volume of more than 2,000 mL; and the nonsevere postpartum hemorrhage group, defined as postpartum bleeding volume of not more than 2,000 mL (*Table 2*) (17). The study was conducted in accordance with the Declaration of Helsinki (as revised in 2013). The study was approved by the Ethical Committee of Southwest Hospital (IRB No. KY2020295). Written informed consent was obtained from the patients for publication of this study and any accompanying images. A copy of the written consent is available for review by the editor-in-chief of this journal.

Inclusion criteria

The inclusion criteria were the following: (I) diagnosis of invasive placenta accreta based on preoperative ultrasound and MRI findings of the placenta attached to an atomic scar combined with a history of previous cesarean delivery; (II) intraoperative or postoperative pathological confirmation of combined IPA; and (III) fulfillment of the diagnostic criteria for postpartum hemorrhage (i.e., bleeding volume ≥1,000 mL 24 h after cesarean section; *Figure 1*).

Exclusion criteria

The exclusion criteria were the following: (I) absence of risk assessment using ultrasound and MRI; (II) intraoperative exploration not consistent with the preoperative diagnosis of IPA; (III) multiple pregnancy; and (IV) high-risk factors for postpartum hemorrhage, such as abnormal coagulation function, severe liver or kidney disease, and excessive accumulation of amniotic fluid (*Figure 1*).

MRI data acquisition

The whole abdomen and pelvis of all patients were scanned preoperatively at our hospital using the Siemens 3T MRI scanner (Siemens Healthineers, Erlangen, Germany) with a 4-channel body-surface coil. At moderate bladder filling, the patients were placed in the supine position with the midsagittal plane perpendicular to the bed surface. Their hands were placed on the head, and both legs were slightly abducted. Images were acquired from the lateral pubic symphysis to the lateral posterior sacral eminence in the sagittal plane and from the upper border of the diaphragm to 20 mm below the anal opening in the transverse plane. The patients were imaged at rest and during the Valsalva maneuver. The fast half-Fourier acquisition single-shot turbo spin-echo sequence was used in the sagittal plane with the following parameters: repetition time, 1,000 ms; echo time, 91 ms; layer thickness, 3–6 mm; layer spacing, 1.2 mm; field of view, 300×300 mm; matrix, 300×256; and bandwidth, 781 Hz/Px. The T2-weighted turbo spin-echo sequence was used in the transverse plane with the following parameters: repetition time, 8610 ms; echo time, 9.8 ms; field of view, 280×280 mm; matrix, 512×512; layer thickness, 2 mm; layer spacing, 0.4 mm; pixel size, 0.55 mm × 0.55 mm; number of excitations, 1; bandwidth, 315 Hz/Px; and

Table 2 Comparison of intraoperative findings between the severe and non-severe postpartum hemorrhage subgroups in all four groups

Variables	Abdominal aortic balloon block (AABB) with peripartum hysterectomy (PH) group			AABB group			PH group			Non-surgical intervention group		
	A	B	P	A	B	P	A	B	P	A	B	P
Blood loss (mL)	4,500±2,041.24	2,000±0	0.060	3,550±2,050.61	1,600±141.42	0.121	5,625±2,561.74	1,750±353.55	0.064	2,982±446.81	1,278±345.61	0.000
Area of the uterus (mm^2)	226,985.5±27,522.35	220,638±18,693.1	0.643	18,7966.5±11,653.83	283,222±44,314.38	0.121	302,082±72,790.99	270,986±9,946.16	1.000	217,906±37,891.46	226,278± 19,812.88	0.558
Area of the placenta (mm^2)	134,415.5±22,033.18	127,829±7,407.65	0.355	12,3048.5±23,441.29	132,888±36,926.53	0.439	148,817±18,689.17	127,502±28,958.85	0.643	122,411±43,007.08	138,918±35,650.26	0.37
Area of placental implantation (mm^2)	39,585.1±10,350.92	36,135.55±2,231.13	0.355	43,810.65±16,956.92	18,776.5±2,077.48	0.121	66,203.8±30,103.56	18,909.5±14,316.93	0.064	31,709±15,280.1	8,505±5,382.81	0.000
Area of placental implantation/area of the placenta	0.2913±0.038	0.2826±0.0011	1.000	0.3759±0.21	0.1492±0.057	0.121	0.4365±0.16	0.1392±0.081	0.064	0.267±0.096	0.067±0.051	0.000
Area of the placenta/area of the uterus	0.5152±0.18	0.5615±0.11	1.000	0.6520±0.084	0.4647±0.058	0.121	0.5152±0.15	0.4689±0.09	1.000	0.558±0.142	0.610±0.131	0.409
Maximum depth of invasion of the placenta (mm)	26.24±5.18	24.03±0.33	0.355	22.28±5.93	11.88±2.14	0.121	34.76±5.91	15.12±0.46	0.064	23.07±10.89	11.13±3.33	0.005
Position of the placenta	4.75±0.96	4±1.41	0.475	5±0	4.5±0.71	0.317	4.25±0.5	4.5±0.71	0.576	4.64±0.67	4.56±0.53	0.773
Score of the implant location	5±0	5±0	1.00	4±2.83	2.5±0.71	0.683	5.25±0.96	2.5 ±0.71	0.060	4.82±0.87	2.67±1.12	0.000
Position of placental implantation (distance from the maximum depth of invasion of the placenta to the cervix; mm)	0±0	0±0	1.00	0±0	70.87 ±45.83	0.102	0±0	29.35 ±41.51	0.157	0.0±0.0	29.4±29.94	0.004
Volume of the uterus (mm^3)	5,334,629.8 ±779,487.43	509,2291.5 ±913,866	0.643	365,4608±321,944.3	5,235,354.5 ±2,959.24	0.121	669,0954±624,032.57	5,841,767±826,352.56	0.165	4,666,573±1,168,280.23	4,945,417±611,966.56	0.527
Volume of the placenta (mm^3)	1,099,546±250,642.41	122,9536.5 ±240,471	0.643	923,892±114,852.53	736,438.5±152,747.09	0.439	113,6141±260,465.46	1,199,082±246,633.89	0.643	893,188±288,627.87	106,5330±267,190.87	0.187
Volume of placental implantation (mm^3)	124,562.4±32,122.32	95,895.9±20,681.6	0.355	135,922.9±63,030.15	37,531.8±15,830.51	0.121	24,1089±151,646.22	43,169.7±29,815.02	0.064	72,785±32,850.06	17,514±14,596.7	0.000

A: severe postpartum hemorrhage subgroup; B: non-severe postpartum hemorrhage subgroup.

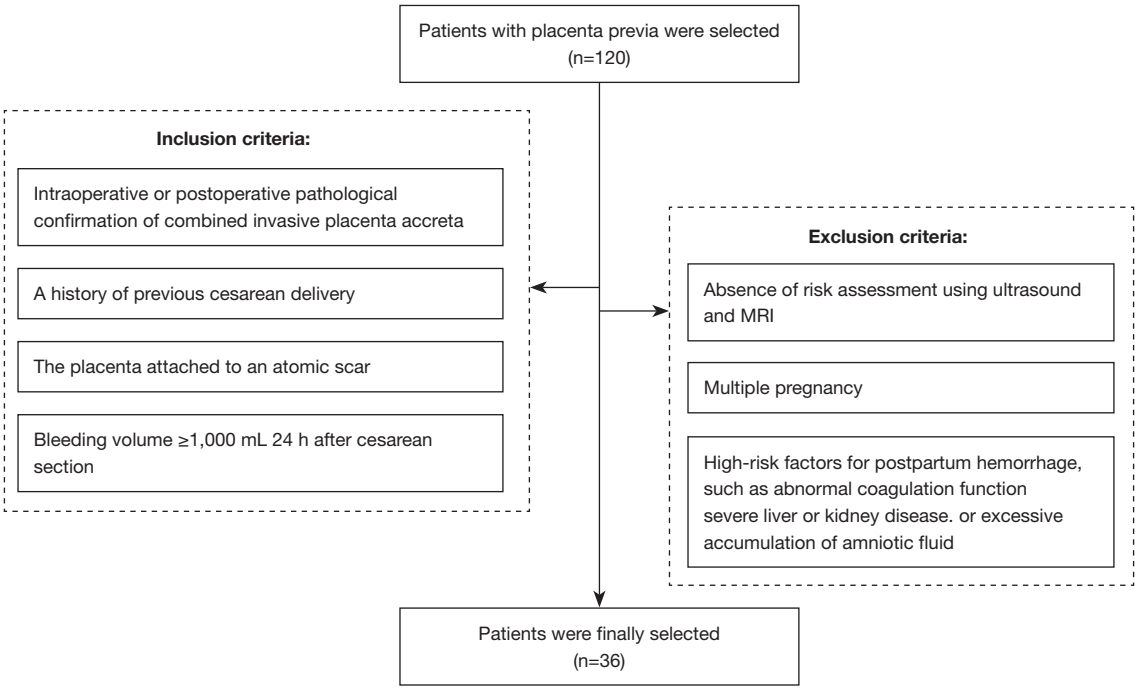

Figure 1 Inclusion and exclusion criteria of IPA patients. MRI, magnetic resonance imaging; IPA, invasive placenta accreta.

acquisition time, approximately 30 min.

MRI image analysis

There are no unified imaging diagnostic criteria for PAS, and the criteria for this study are summarized with reference to reports in the literature (18,19) and the cases in this study as follows: (I) placental augmentation, observed as localized placenta bulge, outward protrusion of the uterine contour at the placental attachment site, and a wider lower uterine segment than the fundus; (II) placental signal heterogeneity, observed as patchy low-signal areas scattered in T2-weighted images; (III) abnormal intraplacental vessels, observed as tortuous, dilated, clustered, and abnormal flow space signals near the myometrial scar; (IV) uterine myometrial thinning/interruption, observed as myometrial thickness <1 mm, an inconspicuous myometrium, or absence of the myometrial signal; (V) intraplacental nodular or band-like low signal on T2-weighted images; and (VI) placental depression, observed as localized, wedge-shaped depression and deformation of the placenta accompanied by a low-signal band.

Three-dimensional modeling and data measurement and comparison

Using Amira 5.2.2 (Visage Imaging, Richmond, Australia) software, the uterus, placenta, IPA, and urinary bladder were segmented separately. The grayscale was adjusted to identify the boundaries of each structure from the clearest plane of each structure to the end of the disappearing plane for manual segmentation to complete the 3D reconstruction. The sagittal and coronal images filtered for the phase favorable for outlining were imported into Amira 5.2.2. After selection of the best plane, the maximum depth of implantation (i.e., the distance from the thickest point of IPA to the cervical opening) was measured using the 3D measurement tool in the software, while the area and volume of the uterus, placenta, and IPA were measured using the area and volume measurement tools in the software. The images of each case were sketched by obstetricians and gynecologists trained in 3D reconstruction sketching and MRI scan recognition and then reviewed by an experienced 3D reconstruction professor and a senior radiologist trained in obstetric MRI scan recognition.

The personnel involved in 3D reconstruction image sketching were blinded to the patients' intraoperative and postoperative conditions.

Statistical analysis

Statistical analyses were performed using SPSS 19.0 (IBM Corp., Armonk, NY, USA) software. Measurement data are expressed as mean ± standard deviation. Each parameter measured in the severe and nonsevere postpartum hemorrhage subgroups was confirmed to be normally distributed. The independent-samples *t*-test was performed for intragroup comparisons. P values <0.05 were considered statistically significant. The receiver operating characteristic (ROC) curve was plotted to analyze the diagnostic values of the area, volume, and depth of IPA in the postpartum hemorrhage of fatal placenta previa with IPA. Areas under the curve (AUC) are always interpreted as the area under the ROC curve. AUC values of <0.5, 0.5–0.7, 0.7–0.9, and >0.9 had no, low, moderate, and high diagnostic values, respectively. Two-sided tests were performed, with an alpha of 0.05.

Results

Study population

We retrospectively enrolled 36 patients in this study. The baseline data did not differ between the severe and nonsevere postpartum hemorrhage subgroups (P<0.05; *Table 1*). The AABB, PH, AABB with PH, and nonsurgical treatment groups comprised 10, 12, 4, and 20 patients, respectively.

Three-dimensional reconstruction of the placenta and IPA

We created a 3D model of 36 cases of IPA. The placental attachment location and area in the model were consistent with those found commonly during cesarean section. The 3D-reconstructed model accurately reflected the postpartum placenta and IPA site, 3D morphology, and spatial adjacency. We present representative cases of all 4 groups below.

AABB with PH group

In the AABB with PH group, a patient (column A in *Figure 2*) had IPA in the anterior uterine wall and cervix involving the urinary bladder, with an implantation area of 51,406 mm^2, implantation volume of 125,722 mm^3, IPA:placental area ratio of 0.333, and postpartum bleeding volume of 6,500 mL. Another patient (column B in *Figure 2*) had IPA in the anterior uterine wall and cervix, with an implantation volume of 150,210 mm^3 and an IPA:placental area ratio of 0.3121. Another patient (column C in *Figure 2*) had IPA in the lower part of the anterior uterine wall, with an implantation volume of 81,271.8 mm^3 and an IPA:placental area ratio of 0.2834.

AABB group

In the AABB group, a patient (column A in *Figure 3*) had IPA in the anterior uterine wall and cervix involving the urinary bladder, with an implantation volume of 180,492 mm^3 and an IPA:placental area ratio of 0.5241. Another patient (column B in *Figure 3*) had IPA in the anterior and posterior uterine walls that did not involve the urinary bladder, with an implantation volume of 91,353.9 mm^3 and an IPA:placental area ratio of 0.22789. Another patient (column C in *Figure 3*) had IPA in the lower anterior part of the right and posterior uterine walls that did not involve the urinary bladder, with an implantation volume of 26,337.98 mm^3 and an IPA:placental area ratio of 0.1089.

PH group

In the PH group, a patient (column A in *Figure 4*) had IPA in the anterior and posterior uterine walls and cervix involving the urinary bladder, with an implantation volume of 455,205 mm^3 and an IPA:placental area ratio of 0.5664. Another patient (column B in *Figure 4*) had IPA in the anterior uterine wall and cervix involving the urinary bladder, with an implantation volume of 138,693 mm^3 and an IPA:placental area ratio of 0.4033. Another patient (column C in *Figure 4*) had IPA in the lower anterior, right, and posterior uterine walls that did not involve the urinary bladder, with an implantation volume of 64,252.1 mm^3 and an IPA:placental area ratio of 0.1962.

Nonsurgical treatment group

In the nonsurgical treatment group, a patient (column A in *Figure 5*) had IPA in the anterior, left, and posterior uterine walls and cervix not involving the urinary bladder, with an implantation volume of 56,987.2 mm^3 and an IPA/placental area ratio of 0.3625. One patient (column B in *Figure 5*) had IPA in the anterior uterine wall and cervix not involving the urinary bladder, with an implantation volume of 41,982.5 mm^3 and an IPA:placental area ratio of 0.1391. Another patient (column C in *Figure 5*) had IPA in the

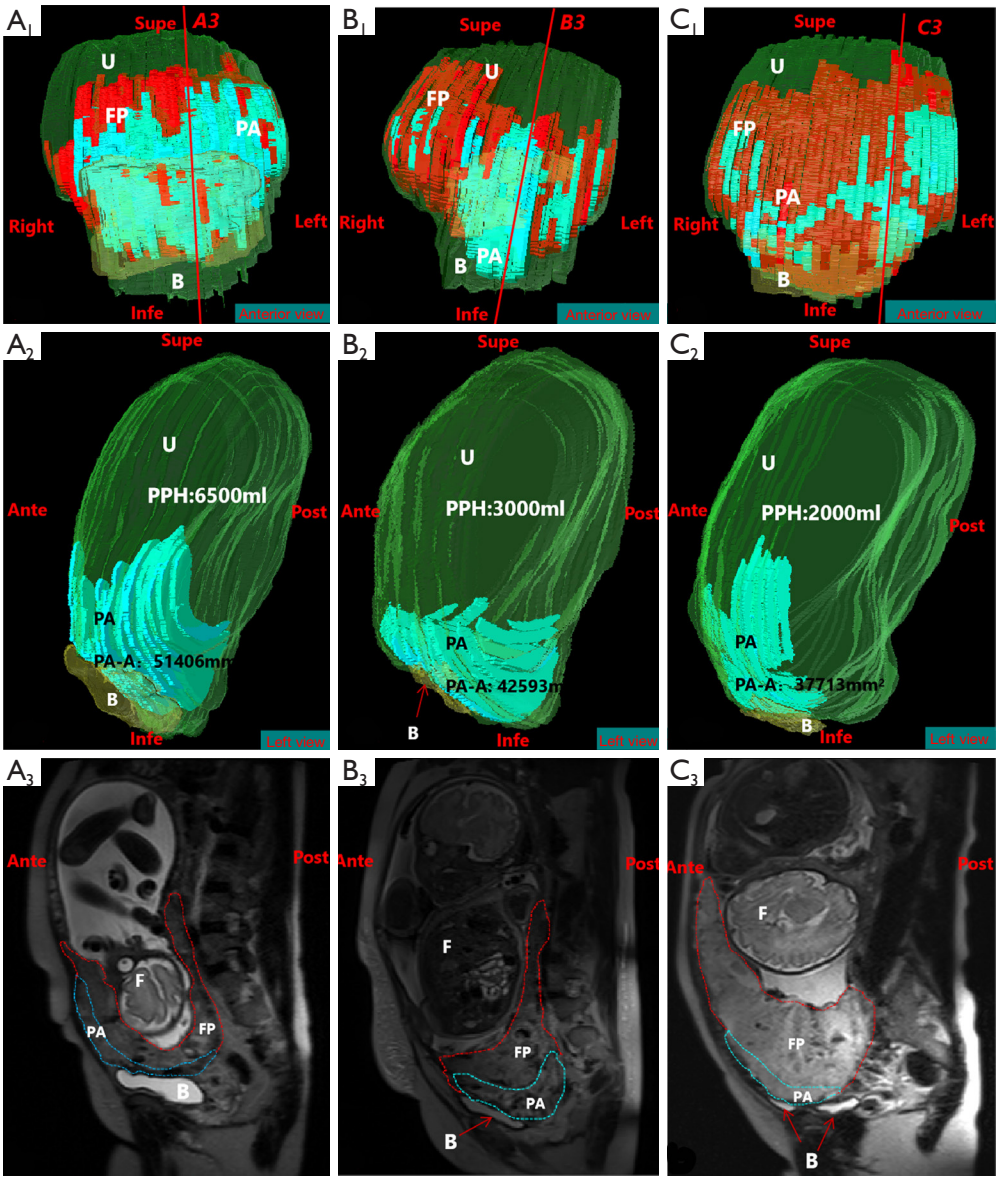

Figure 2 Three-dimensional reconstructions of MRI of a patient in the abdominal aortic balloon block with the peripartum hysterectomy group. (A1-C1) show the anterosuperior view; (A2-C2) show the left lateral views; and (A3-C3) show the sagittal views. B, urinary bladder (yellow); U, uterus (green); FP, placenta (red); PA, IPA (blue); F, fetus; Supe, superior; Infe, inferior; Ante, anterior; Post, posterior; PA-A, area of IPA; PPH, postpartum hemorrhage; MRI, magnetic resonance imaging.

lower anterior uterine wall and cervix, with an implantation volume of 49,284.6 mm^3 and an IPA:placental area ratio of 0.2243. One patient (column D in *Figure 5*) had IPA in the anterior uterine wall, with an implantation volume of 81,271.8 mm^3, an IPA:placental area ratio of 0.0313, and a postpartum bleeding volume of 1,200 mL. Finally, one patient (column E in *Figure 5*) had IPA in the anterior uterine wall, with an implantation volume of 6,693.74 mm^3 and an IPA:placental area ratio of 0.024.

Statistical analysis

Table 2 shows that the mean IPA area, IPA area:placental area ratio, maximum depth of IPA location score, and IPA volume were significantly higher in the severe postpartum hemorrhage subgroup than in the nonsevere postpartum

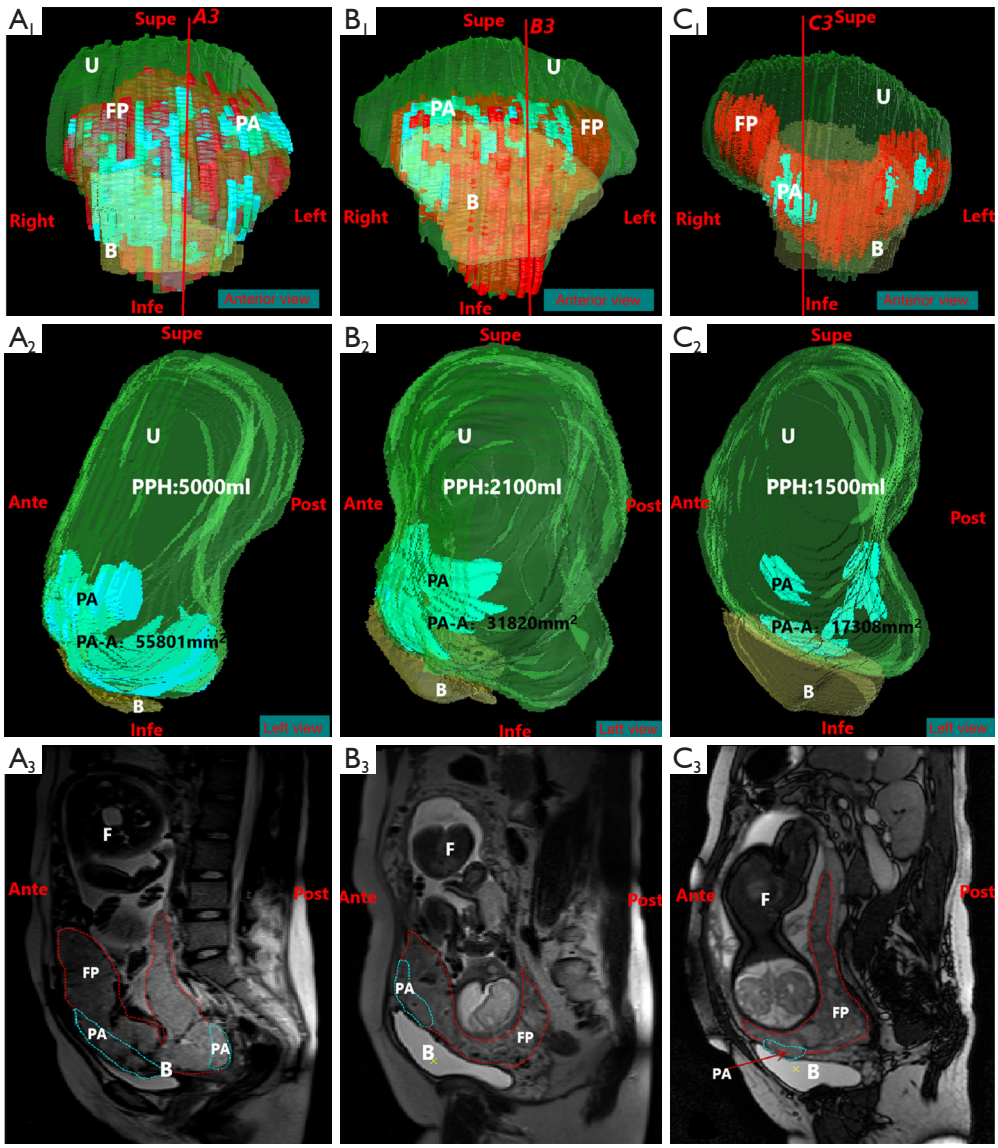

Figure 3 Three-dimensional reconstructions of magnetic resonance imaging of a patient in the abdominal aortic balloon block group. (A1-C1) show the anterosuperior view; (A2-C2) show the left lateral view; and (A3-C3) show the sagittal view. B, urinary bladder (yellow); U, uterus (green); FP, placenta (red); PA, IPA (blue); F, fetus; Supe, superior; Infe, inferior; Ante, anterior; Post, posterior; PA-A, area of IPA; PPH, postpartum hemorrhage.

hemorrhage subgroup in the nonsurgical treatment group ($P<0.05$) but did not differ significantly between the 2 subgroups in any other group ($P>0.05$), probably because of the small sample size of the other groups.

Tables 3,*4* show that the AUCs of the implantation area, implantation volume, maximum depth of implantation, and implantation area:placental area ratio exceeded 0.9 and strongly correlated with severe postpartum hemorrhage, while those of the uterine area, uterine volume, placental area, placental volume, and placental area:uterine area ratio were between 0.5 and 0.7 and correlated with severe postpartum hemorrhage.

The threshold (cutoff points) determining severe postpartum hemorrhage were 20,286.25 mm^2 for the implantation area, 0.01271 for the implantation area:placental area ratio, 15.03 mm for the maximum depth of implantation,

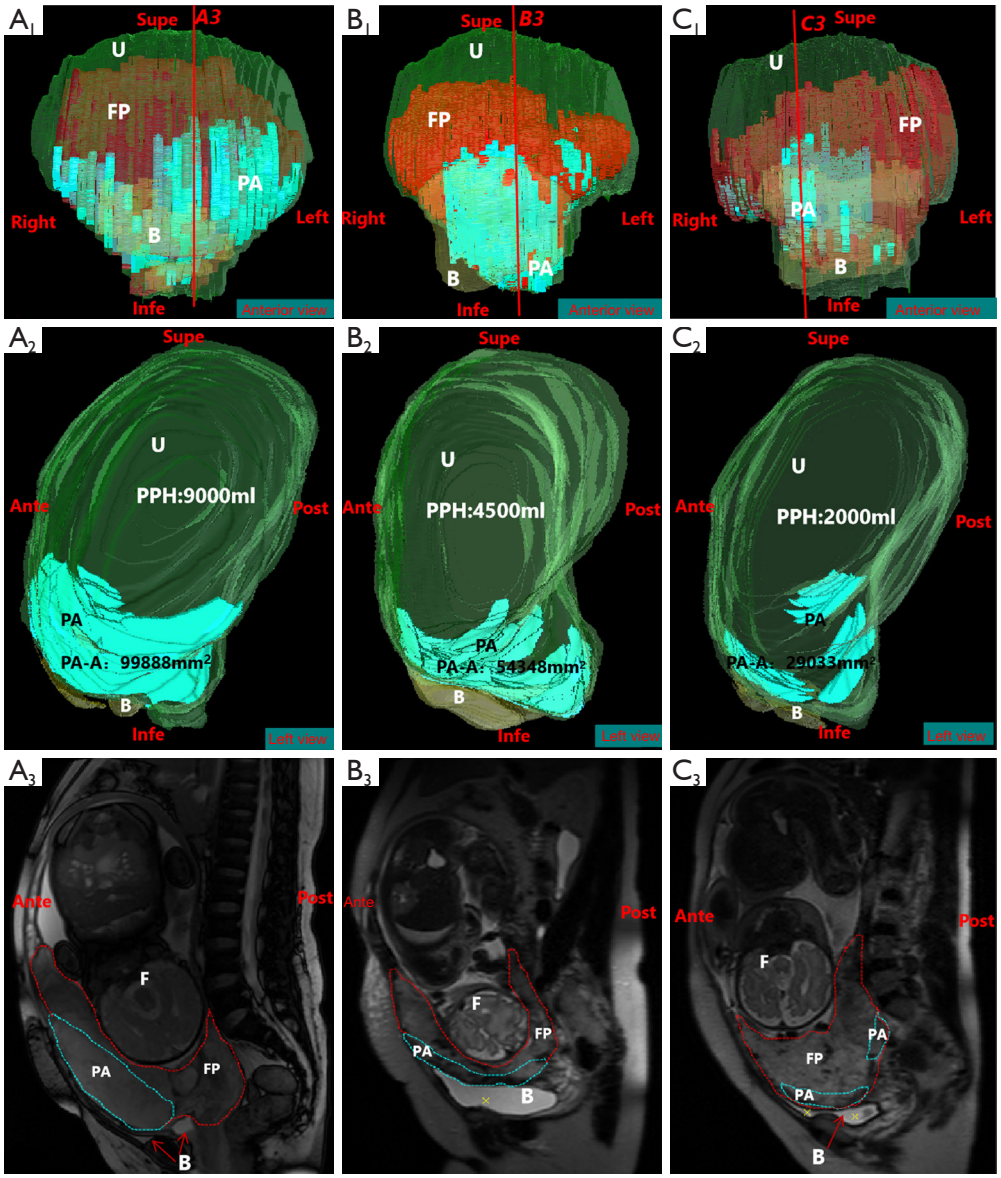

Figure 4 Three-dimensional reconstructions of magnetic resonance imaging scans of a patient in the peripartum hysterectomy group. (A1-C1) show the anterosuperior views; (A2-C2) show the left lateral views; and (A3-C3) show the sagittal views. B, urinary bladder (yellow); U, uterus (green); FP, placenta (red); PA, IPA (blue); F, fetus; Supe, superior; Infe, inferior; Ante, anterior; Post, posterior; PA-A, area of IPA; PPH, postpartum hemorrhage.

and 46,846 mm^3 for the implantation volume (*Figure 6*).

Discussion

Clinical and research implications of MRI-based 3D reconstruction of IPA and its adjacent structures

Imaging-based 3D reconstruction and visualization have been widely used in hepatology, orthopedics, and obstetrics and gynecology (20,21). Three-dimensional reconstruction and visualization of the liver is a safe and effective method for the accurate diagnosis, preoperative assessment, surgical planning, and postpartum precision guidance of liver tumors, shortening the operating time and reducing postpartum bleeding. The Department of Digital Medicine

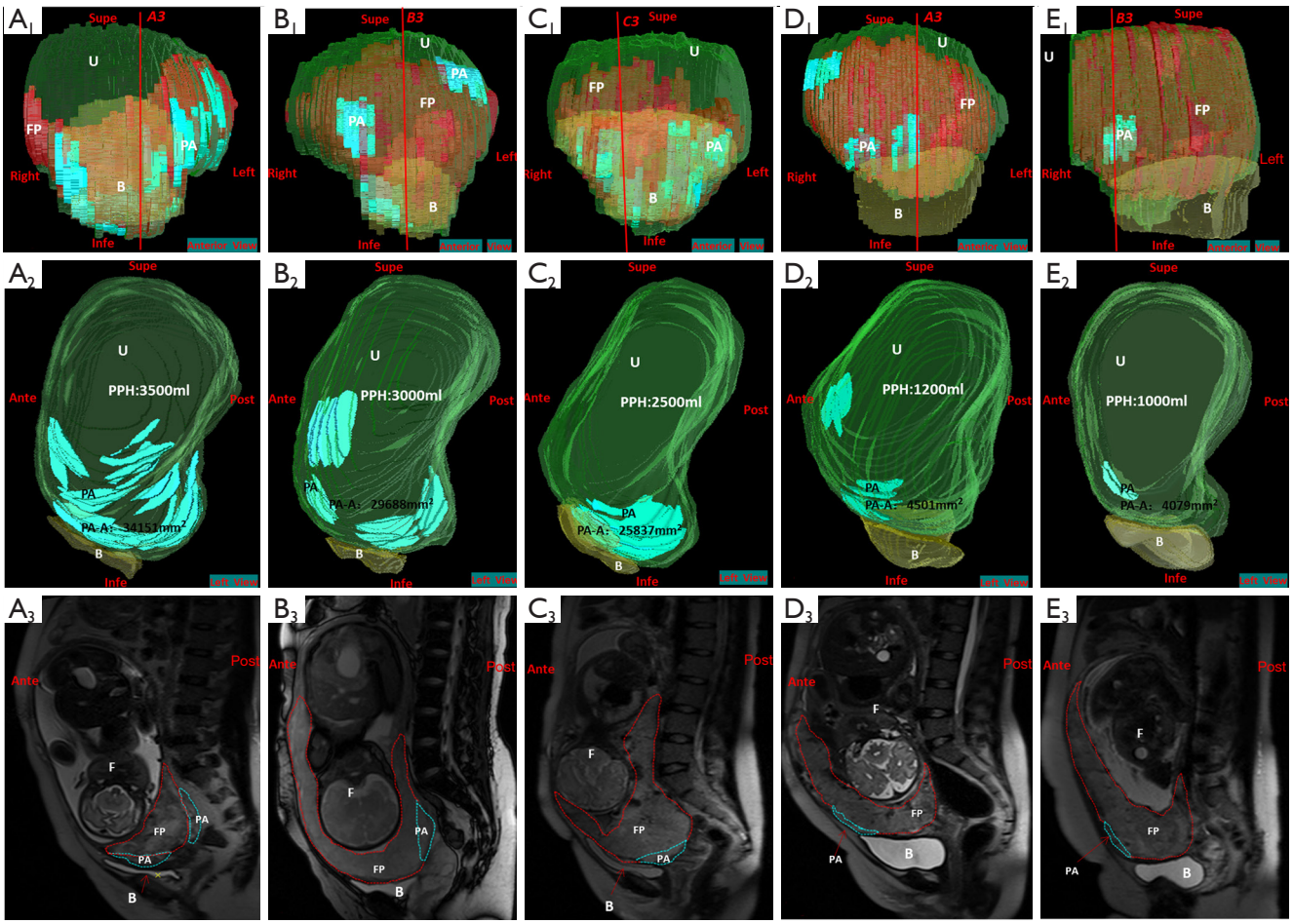

Figure 5 Three-dimensional reconstructions of magnetic resonance imaging of a patient in the nonsurgical treatment group. (A1-E1) show the anterosuperior views; (A2-E2) show the left lateral views; and (A3-E3) show the sagittal views. B, urinary bladder (yellow); U, uterus (green); FP, placenta (red); PA, IPA (blue); F, fetus; Supe, superior; Infe, inferior; Ante, anterior; Post, posterior; PA-A, area of IPA; PPH, postpartum hemorrhage.

at Army Medical University used 3D reconstruction technology based on CT, MRI, and thin-sectional, high-resolution anatomical images in the cardiovascular system, bones, and pelvic floor. Wu *et al.* performed 3D reconstruction and visualization of complicated mediastinal tumors to accurately diagnose disease, improve surgical precision, and reduce surgical complications (22-25).

In our study, 3D reconstruction of MRI images of the IPA and its adjacent structures, including the placenta, uterus, and bladder, were performed. The implanted part of the placenta was segmented separately and clearly to demonstrate the location of IPA, its 3D morphology, and spatial relationship, enabling the accurate localization of IPA and measurement of the implantation depth, area, and volume. The 3D model demonstrated the location, depth, area, and volume of IPA and its relationship with adjacent structures, including invasion of the bladder, which could be used to guide preoperative surgical planning and accurate treatment decision-making. Indications for uterine suturing for hemostasis and partial or complete hysterectomy are identified based on the location, size, depth, area, and volume of IPA combined with postpartum bleeding volume. If the implanted area is larger and the implantation depth is deeper or invades the bladder, active hysterectomy can be life-saving surgery and a good management decision. If the IPA invades the bladder, urological assistance can be requested to avoid bladder and urethral injury and conduct a vesicovaginal fistula as soon as possible (26).

Table 3 Receiver operating characteristic curve

Morphological parameters	Area under the curve (AUC)	Sensitivity	Specificity	Critical value
Area of the uterus	0.606	0.889	0.455	205,222
Area of the placenta	0.657	0.889	0.455	109,411.5
Volume of the uterus	0.586	0.889	0.364	4,210,407
Volume of the placenta	0.697	0.889	0.636	839,450.5
Area of the placenta/area of the uterus	0.646	0.556	0.818	0.6535

Table 4 Area under the curve (AUC)

Morphological parameters	AUC	Sensitivity	Specificity	Critical value
Area of placental implantation	0.990	0.909	1.00	20,286.25
Area of placental implantation/area of the placenta	0.970	1.00	0.889	0.1271
Maximum depth of invasion of the placenta	0.960	0.909	0.889	15.03
Volume of placental implantation	0.990	0.909	1.00	46,846

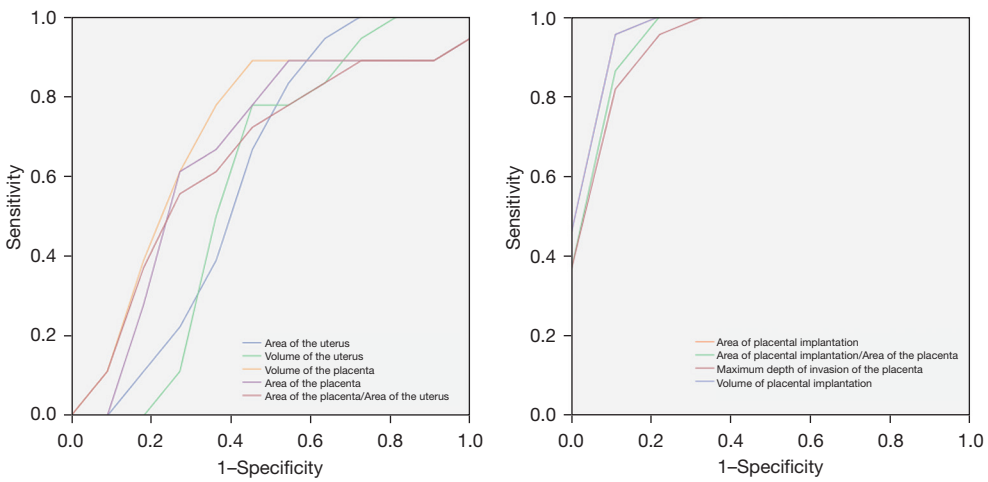

Figure 6 A multifactorial unconditional logistic regression analysis of 3D morphological parameters and severe postpartum hemorrhage. In the right figure, the lines of area of placental implantation and volume of placental implantation overlap.

Morphological parameters for the risk assessment of severe postpartum hemorrhage using MRI-based 3D reconstruction

In this study, the depth, volume, and area of IPA and implanted area:placental area ratio were closely associated with the risk of severe postpartum hemorrhage. Similarly, Mulligan *et al.* showed that the deeper, larger, and more voluminous the implantation is, the more likely is the occurrence of damage during detachment and, consequently, the occurrence of severe hemorrhage (16). We calculated the threshold (cutoff value) of the depth, area, and volume of IPA, which could be used to more accurately predict severe hemorrhage and help reduce surgery complications.

Advances in 3D imaging features of the placenta and IPA

The risk of postpartum hemorrhage from IPA is evidently higher than that from cesarean delivery alone. Conventional ultrasound and MRI assess the risk of postpartum hemorrhage and adjacent organ involvement,

with a sensitivity of approximately 85–95% (27). Inaccurate assessment leads to the requirement of a postpartum passive hysterectomy with potentially severe bladder or urethral injury, which is associated with high morbidity and economic burden. Therefore, 3D technology can compensate for the shortcomings of conventional ultrasound and MRI and allow for the accurate demonstration of the lesion and its adjacent structures.

He *et al.* (28) reported a case of complex placental implantation in a pregnant woman during cesarean section detected by a preoperative MRI 3D reconstruction. Transposterior hysterectomy was performed with precise and complete removal of the uterus. However, the study was only a case report and did not explore the correlation of the depth, area, volume, or degree of IPA with severe postpartum hemorrhage.

Cao *et al.* (29) showed that a digital 3D model of the placenta assisted the surgical plan of the uterine incision, effectively avoiding IPA and shortening the operative time. However, only the pelvis, uterus, and placenta were 3-dimensionally reconstructed, and the model did not include the location, 3D morphology, or spatial relationships of IPA, nor did it include the determination of the risk factors of postpartum hemorrhage in IPA. In our study, we created detailed anatomical information about the IPA, which help to assess bleeding, evaluate the operative risk, and improve surgical precision.

Chen *et al.* (13) measured the IPA depth, area, and length using 2D MRI and ultrasound and a multifactorial regression analysis of clinical data and concluded that IPA strongly correlated with severe postpartum hemorrhage. However, the accuracy of the results was limited by the small sample size of clinical data and the use of 2D imaging to measure the IPA. Our study quantified the implantation depth, area, and volume of IPA in 3D, which is superior to 2D quantification.

Limitations

This study had some limitations. Firstly, the sample size was small because the MRI of IPA was not easy to acquire. Secondly, the study design was retrospective, leading to a selection bias. Thirdly, this was a single-center study, and thus the generalizability of the results is restricted. Fourth, myometrial thinning/interruption might not have been judged accurately because the surfaces of the uterine scars were not smooth after cesarean section, leading to the blurring of the MRI display of the interface between the myometrium and the placenta. Therefore, further development of our study is required through multicenter clinical studies with larger sample sizes.

Conclusions

In conclusion, MRI is a continuous, 2D, tomographic imaging modality. Compared to ultrasound, it has advantages of easier creation of 3D reconstruction models, accurate quantification of parameters, better display of 3D structures, and more accurate risk assessment results in IPA, thereby making it worthy of clinical application.

Acknowledgments

Funding: This work was supported by the National Natural Science Foundation of China (No. 31971113), the Chongqing Science and Technology Talent Project (No. CQYC201905037), the University Talent Project (No. XZ2019505029), the Post Graduate Teaching Reform Project in Chongqing (No. yjg183144), and the Accurate Assessment of The Risk of Obstetric Hemorrhage from Anterior Placenta and Graded Treatment (No. cstc2019jscx-msxmX0165).

Footnote

Reporting Checklist: The authors have completed the STARD reporting checklist. Available at https://atm.amegroups.com/article/view/10.21037/atm-22-2940/rc

Data Sharing Statement: Available at https://atm.amegroups.com/article/view/10.21037/atm-22-2940/dss

Conflicts of Interest: All authors have completed the ICMJE uniform disclosure form (available at https://atm.amegroups.com/article/view/10.21037/atm-22-2940/coif). The authors have no conflicts of interest to declare.

Ethical Statement: The authors are accountable for all aspects of the work in ensuring that questions related to the accuracy or integrity of any part of the work are appropriately investigated and resolved. The study was conducted in accordance with the Declaration of Helsinki (as revised in 2013). The study was approved by the Ethical Committee of Southwest Hospital (IRB No. KY2020295). Written informed consent was obtained from the patients for publication of this study and any accompanying images. A copy of the written consent is available for review by the

editor-in-chief of this journal.

References

1. Collins SL, Alemdar B, van Beekhuizen HJ, et al. Evidence-based guidelines for the management of abnormally invasive placenta: recommendations from the International Society for Abnormally Invasive Placenta. Am J Obstet Gynecol 2019;220:511-26.
2. Jauniaux E, Ayres-de-Campos D, Langhoff-Roos J, et al. FIGO classification for the clinical diagnosis of placenta accreta spectrum disorders. Int J Gynaecol Obstet 2019;146:20-4.
3. Marcellin L, Delorme P, Bonnet MP, et al. Placenta percreta is associated with more frequent severe maternal morbidity than placenta accreta. Am J Obstet Gynecol 2018;219:193.e1-9.
4. D'Arpe S, Franceschetti S, Corosu R, et al. Emergency peripartum hysterectomy in a tertiary teaching hospital: a 14-year review. Arch Gynecol Obstet 2015;291:841-7.
5. Kabiri D, Hants Y, Shanwetter N, et al. Outcomes of subsequent pregnancies after conservmive treatment for placenta accrete. Int J Gynaecol Obstet 2014;127:206-10.
6. Brown BP, Meyers ML. Placental magnetic resonance imaging Part II: placenta accreta spectrum. Pediatr Radiol 2020;50:275-84.
7. Pagani G, Cali G, Acharya G, et al. Diagnostic accuracy of ultrasound in detecting the severity of abnormally invasive placentation: a systematic review and meta-analysis. Acta Obstet Gynecol Scand 2018;97:25-37.
8. Kilcoyne A, Shenoy-Bhangle AS, Roberts DJ, et al. MRI of Placenta Accreta, Placenta Increta, and Placenta Percreta: Pearls and Pitfalls. AJR Am J Roentgenol 2017;208:214-21.
9. D'Antonio F, Iacovella C, Palacios-Jaraquemada J, et al. Prenatal identification of invasive placentation using magnetic resonance imaging: systematic review and meta-analysis. Ultrasound Obstet Gynecol 2014;44:8-16.
10. Lum M, Tsiouris AJ. MRI safety considerations during pregnancy. Clin Imaging 2020;62:69-75.
11. Knight JC, Lehnert S, Shanks AL, et al. A comprehensive severity score for the morbidly adherent placenta: combining ultrasound and magnetic resonance imaging. Pediatr Radiol 2018;48:1945-54.
12. Meng LS, Yang ZQ, Yan Y, et al. The application value of Likert scale's scoring system in predicting the depth of placental implantation by MRI. China Medical Equipment 2020;17:79-84.
13. Chen YL, Song T, Liu Y, et al. Diagnostic value of prenatal MRI in placental implantation. Chinese Journal of Medical Imaging 2015;6:470-7.
14. Chen L, Chen M, Pei XL, et al. Value of MRI sign-based scoring model for predicting invasive placental implantation and adverse clinical outcome. Chinese Journal of Perinatal Medicine 2021;24:32-9.
15. Sentilhes L, Kayem G, Chandraharan E, et al. FIGO consensus guidelines on placenta accreta spectrum disorders: Conservative management. Int J Gynaecol Obstet 2018;140:291-8.
16. Mulligan KM, Bartels HC, Armstrong F, et al. Comparing three-dimensional models of placenta accreta spectrum with surgical findings. Int J Gynaecol Obstet 2022;157:188-97.
17. Munoz JL, Blankenship LM, Ramsey PS, et al. Importance of the gynecologic oncologist in management of cesarean hysterectomy for Placenta Accreta Spectrum (PAS). Gynecol Oncol 2022;166:460-4.
18. Sato T, Mori N, Hasegawa O, et al. Placental recess accompanied by a T2 dark band: a new finding for diagnosing placental invasion. Abdom Radiol (NY) 2017;42:2146-53.
19. Budorick NE, Figueroa R, Vizcarra M, et al. Another look at ultrasound and magnetic resonance imaging for diagnosis of placenta accreta. J Matern Fetal Neonatal Med 2017;30:2422-7.
20. Hu M, Hu H, Cai W, et al. The Safety and Feasibility of Three-Dimensional Visualization Technology Assisted Right Posterior Lobe Allied with Part of V and VIII Sectionectomy for Right Hepatic Malignancy Therapy. J Laparoendosc Adv Surg Tech A 2018;28:586-94.
21. Liu P, Chen R, Chen C, et al. Comparison of levator ani muscles in three-dimensional MRI-based models in women with and without pelvic organ prolapse at rest. Zhonghua Fu Chan Ke Za Zhi 2015;50:428-33.
22. Zhong C, Guo Y, Huang H, et al. Three-dimensional reconstruction of coronary arteries and its application in localization of coronary artery segments corresponding

to myocardial segments identified by transthoracic echocardiography. Comput Math Methods Med 2013;2013:783939.
23. Dai C, Guo L, Yang L, et al. Regional fibrocartilage variations in human anterior cruciate ligament tibial insertion: a histological three-dimensional reconstruction. Connect Tissue Res 2015;56:18-24.
24. Wu Y, Chen N, Xu Z, et al. Application of 3D printing technology to thoracic wall tumor resection and thoracic wall reconstruction. J Thorac Dis 2018;10:6880-90.
25. Tan D, Yao J, Hua X, et al. Application of 3D modeling and printing technology in accurate resection of complicated thoracic tumors. Ann Transl Med 2020;8:1342.
26. Kassem GA, Alzahrani AK. Maternal and neonatal outcomes of placenta previa and placenta accreta: three years of experience with a two-consultant approach. Int J Womens Health 2013;5:803-10.
27. Maher MA, Abdelaziz A, Bazeed MF. Diagnostic accuracy of ultrasound and MRI in the prenatal diagnosis of placenta accreta. Acta Obstet Gynecol Scand 2013;92:1017-22.
28. He H, Lin L, Chen DJ. The value of 3D printing model in hysterectomy of patients with complex placental implantation. Chinese Journal of Practical Gynecology and Obstetrics 2014;5:366-8.
29. Cao Y, Wei Y, Yu Y, et al. Safety and efficacy of a novel three-dimensional magnetic resonance imaging model for uterine incision in placenta previa. Int J Gynaecol Obstet 2017;28:336-41.

Cite this article as: Liu L, Yan X, Liu J, Yan P, Du M, Wang R, Wu Y, Wang D. Risk assessment of severe postpartum hemorrhage after invasive placenta accreta based on three-dimensional reconstruction of magnetic resonance imaging. Ann Transl Med 2023;11(1):8. doi: 10.21037/atm-22-2940

